AN IMPROVED PASSIVE SCALAR MODEL FOR HAZARDOUS H_2-AIR IGNITION PREDICTION

M. Le Boursicaud[1], S. Zhao[1], J.-L. Consalvi[2], P. Boivin[1]

[1]**Aix Marseille Univ, CNRS, Centrale Marseille, M2P2, Marseille, France**

[2]**Aix Marseille Univ, CNRS, IUSTI, Marseille, France**

Abstract

As hydrogen becomes an increasingly popular alternative fuel for transportation, the need for tools to predict ignition events has grown. Recently, a cost-effective passive scalar formulation has been developed to address this need [1]. This approach employs a self-reacting scalar to model the hydrogen-air chain-branched explosion (due to reactions of the type *Reactant + Radical* $\rightarrow$ *Radical + Radical*). The scalar branching rate is derived analytically from the kinetic Jacobian matrix [2]. The method accurately reproduces ignition delays obtained by detailed chemistry for temperatures above crossover, where branching is the dominant process. However, for temperatures below the crossover temperature, where other phenomena like thermal runaway are more significant, the scalar approach fails to predict ignition events correctly. Therefore, modifications to the scalar framework have been made to extend its validity across the entire temperature range. Additionally, a simple technique for approximating the molecular diffusion of the scalar has been developed using the eigenvector of the Jacobian, which accounts for differences in the radical pool's composition and non-unity Lewis number effects. The complete modified framework is presented, and its capability is evaluated in canonical scenarios and a more challenging double mixing layer.

1. INTRODUCTION

Hydrogen is considered to be a promising energy carrier for various applications, including aviation. Airbus ZERO-e program aims to fly a 100% H2-powered aircraft by 2035, which raises concerns about hydrogen safety. While hydrogen explosion limits [3] are well-understood, ignition risk is the primary safety concern. Analytical expression of the characteristic ignition delay can already be found in the literature (see, e.g. [4]). Previous studies have shown that the characteristic times associated with ignition are much larger than those associated with H2 flames, making it possible to build reduced chemical descriptions that accurately reproduce ignition without including the short time scales involved in H2 flames. In a previous study, a passive scalar η was introduced to represent intermediate species relevant for hydrogen ignition, and a model was developed to predict ignition for a fraction of the cost of the full reactive simulation. The evolution of η is governed by a classical advection-diffusion-reaction equation:

$$\frac{\partial \rho \eta}{\partial t} + \frac{\partial \rho u_\alpha \eta}{\partial x_\alpha} = \frac{\partial}{\partial x_\alpha}\left(\rho D_\eta \frac{W_\eta}{W}\frac{\partial}{\partial x_\alpha}\left(\frac{W}{W_\eta}\eta\right)\right) + \dot{\omega}_\eta \tag{1}$$

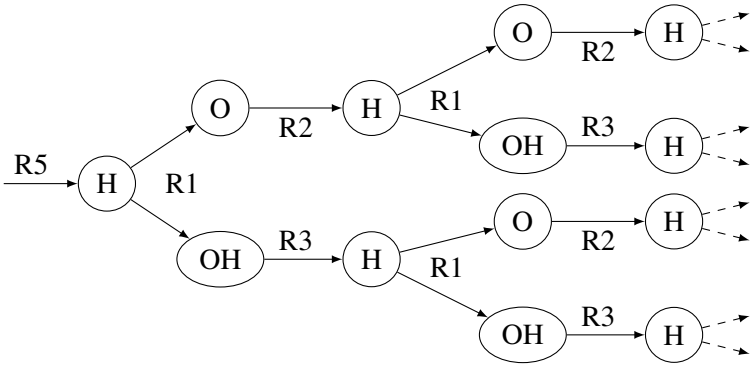

Figure 1: Chain-branching of the high-temperature hydrogen ignition regime, caused by reaction 1, 2 and 3.

However, this model only accurately predicted ignition hazards above crossover. This paper aims to extend and improve the formulation by modifying the source term $\dot{\omega}_\eta$ and the diffusion coefficient D_η to predict ignition hazards for all temperatures, including close or below crossover. The article is organized as follows: Section 2 introduces the necessary notations and recalls the derivation of $\dot{\omega}_\eta$ used in the previous model, Section 3 extends the formulation to take into account thermal runaway responsible for ignition at low temperatures or high pressures and investigates the effect of the radical pool diffusion properties through D_η, Section 4 investigate the performance of the scalar for a turbulent mixing layer and the article closes with conclusions and perspectives.

2. THE IGNITION SCALAR MODEL

2.1. Minimal hydrogen ignition description

To start, we need to identify the necessary reactions to represent the ignition process for a wide range of temperatures and pressure. Previous studies [2, 5, 6] point out that the skeletal mechanism composed of the following 8 steps are enough:

Table 1: Chemical reactions responsible for hydrogen ignition. Rates numerical values can be found in the up-to-date San Diego mechanism [7].

1	$H+O_2 \rightarrow OH+O$	5	$H_2+O_2 \rightarrow HO_2+H$
2	$H_2+O \rightarrow OH+H$	6	$2HO_2 \rightarrow H_2O_2+O_2$
3	$H_2+OH \rightarrow H_2O+H$	7	$HO_2+H_2 \rightarrow H_2O_2+H$
4	$H+O_2+M \rightarrow HO_2+M$	8	$H_2O_2+M \rightarrow 2OH+M$

Among these 8 reactions, we found the classical branching (1-3) illustrated in Figure 1, termination (4), and initiation steps (5) already known to be essential for ignition in the high-temperature regime [8, 9]. Reactions (6-8) have additionally been identified to be responsible for the low-temperature ignitions [5, 8] and the third explosion limit [10]. This 8-step mechanism has already been validated for a wide range of pressure/temperature [2].

The so-called crossover delimits two regimes in the pressure and temperature domain, depending on whether H-consumption through reaction 1 or 4 is dominant. In the former case, the H-atom production increases exponentially as described in Fig. 1 via R1, R2, and R3. In the latter case, R4 is dominant and acts as a sink for H, preventing the chain-branching process.

Hereafter, we use the classical definition of the hydrogen ignition crossover [4], defined as the condition

for which reaction 1 is half of the rate of reaction 4. A crossover parameter α is introduced then as:

$$\alpha = \frac{2k_1}{k_4 C_{\mathrm{M4}}}, \tag{2}$$

where k_1 and k_4 represent the rate constants of reactions 1 and 4, while C_{M4} is the third body concentration associated with reaction 4, as found in the San Diego mechanism: $C_{\mathrm{M4}} = \sum_{k=0}^{N_{sp}} C_k + \frac{3}{2}C_{\mathrm{H_2}} + 15C_{\mathrm{H_2O}}$.

The crossover is therefore defined as $\alpha = 1$. α depends essentially on the pressure (via C_{M4}) and temperature (via Arrhenius constants k_i). For a given pressure, the temperature for which $\alpha = 1$ is the crossover temperature T_c.

With this definition, the above crossover or high-temperature regime is defined by $\alpha > 1$, where the radical pool primarily consists of H, O and OH; while the low-temperature, or below-crossover regime ($\alpha < 1$) is dominated by HO_2, and H_2O_2 species.

2.2. Recap and notations

The radicals of the hydrogen chemistry consist of the 5 species previously named, H, O, OH, HO_2, and H_2O_2. By writing their concentrations in a vectorial form:

$$\bar{C} = \begin{bmatrix} C_{\mathrm{H}} & C_{\mathrm{O}} & C_{\mathrm{OH}} & C_{\mathrm{HO_2}} & C_{\mathrm{H_2O_2}} \end{bmatrix}^T, \tag{3}$$

their production rates can be written with a linear system:

$$\frac{\mathrm{d}\bar{C}}{\mathrm{d}t} = \mathbf{A}\bar{C} + \bar{\epsilon}. \tag{4}$$

where $\mathbf{A}$ is the chemical Jacobian matrix, and $\bar{\epsilon}$ is an initial rate vector. Neglecting step 6, they read

$$\mathbf{A} = \begin{bmatrix} -l_1 - l_4 & l_2 & l_3 & l_7 & 0 \\ l_1 & -l_2 & 0 & 0 & 0 \\ l_1 & l_2 & -l_3 & 0 & 2l_8 \\ l_4 & 0 & 0 & -l_7 & 0 \\ 0 & 0 & 0 & l_7 & -l_8 \end{bmatrix}, \; \bar{\epsilon} = \begin{bmatrix} \omega_5 \\ 0 \\ 0 \\ \omega_5 \\ 0 \end{bmatrix}. \tag{5}$$

here ω_5 is the rate of reaction 5 (e.g. $\omega_5 = k_5 C_{\mathrm{O_2}} C_{\mathrm{H_2}}$) as given in Tab. 1, and the l_k correspond to the inverse characteristic time (e.g. $l_1 = k_1 C_{\mathrm{O_2}}$) of the k^{th} reaction, which only depends on temperature, pressure, and major species (H_2, O_2, and diluent). The system (3) can be solved analytically when the temperature and main reactants (H_2, O_2) can be assumed to be constant (e.g. $\mathbf{A}$ is a constant) throughout the ignition process, like in an isobaric homogeneous reactor.

System (4), through diagonalization of $\mathbf{A}$ (5) and the rapid dominance of its largest eigenvalue λ, may be represented by a simple scalar C_η evolution equation:

$$\frac{\mathrm{d}C_\eta}{\mathrm{d}t} = \lambda C_\eta + \epsilon_\eta. \tag{6}$$

For the present study, $\epsilon_\eta = \omega_5$ have been retained for simplicity, leading to $C_\eta \approx C_{\mathrm{H}}$ above crossover and $C_\eta \approx C_{\mathrm{HO_2}}$ at low temperature. Those properties will be used later on for the new framework.

The scalar concentration C_η [molar concentration] is related to η [mass fraction] of Eq. (1) with $C_\eta = \rho\eta/W_\eta$, where W_η is a molecular weight given for η. As it will be discussed later, any choice of W_η will lead to the same ignition events because the ignition criteria will be based on C_η. Finally, the scalar production rate $\dot{\omega}_\eta$ present in (1) reads:

$$\dot{\omega}_\eta = \left(\lambda C_\eta + \epsilon_\eta\right) W_\eta. \tag{7}$$

The comparison between the evolution of C_η and C_H is shown in Figure 2.a for an isobaric homogeneous reactor initially containing a stoichiometric H_2-air mixture at p=1 atm and T_0=1100 K (above crossover). The normalized temperature $\Theta = (T - T_0)/(T_{max} - T_0)$ is also displayed.

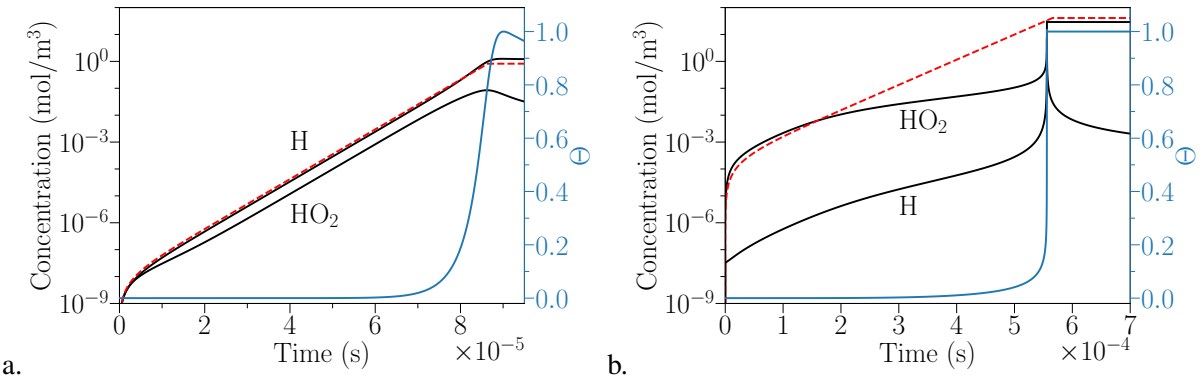

Figure 2: Normalized temperature (blue line, right axis), H and HO_2 concentrations (black lines, left axis) as functions of time, during isobaric homogeneous ignition processes from numerical integration with the 8-step skeletal chemistry for φ=1.0, with p=1 atm, T_0=1100 K ($> T_c$, left) and p=50 atm, T_0=1100 K ($< T_c$, right). C_η is also presented, until it reaches the limiting reactant concentration $C_\eta = \min(C_{\mathrm{H}_2}, C_{\mathrm{O}_2}/2)$ (red dashed).

From the integration of Eq. (6), C_η follow closely the evolution of C_H even without considering heat release, it is also clear that $C_\eta = \min(C_{\mathrm{H}_2}, C_{\mathrm{O}_2}/2)$, materialised by the C_η curve horizontal level, is an adequate ignition condition.

In 2.b, the same has been done for conditions relevant to hydrogen storage, by keeping the same temperature (T_0=1100 K) and using a higher pressure of p=50 atm (below crossover). C_η follows the evolution of C_{HO_2}, but only in the first stage of ignition. Indeed, reaction 6 is missing when computing $\dot{\omega}_\eta$, and it's this reaction that is slowing down the branching process by producing only one radical while destroying two of them. As the crossover temperature increase with pressure (second explosion limit), the framework needs to be modified to properly model the process of ignition for hydrogen storage conditions.

3. AN IMPROVED SCALAR MODEL

The process leading to ignition at temperatures below the cross-over temperature may appear simpler than at high temperatures because the radicals H, O, and OH can be assumed to be in a quasi-steady-state [5]. However, the chemical pathway followed by HO_2 and H_2O_2 highlights the importance of the non-linear branching reaction 6 and the thermal runaway [8]. Therefore, improving the description of ignition close to and below the crossover temperature ($\alpha \lesssim 1$) requires (i) including step 6 in the reaction rate $\dot{\omega}_\eta$ and (ii) taking into account the thermal runaway, which was neglected here because η production does not yield any heat release. In addition, the radicals present in the two regimes have different diffusion properties, we also need (iii) to model the scalar diffusion coefficient. The next three subsections will discuss these points in detail.

3.1. The non-linearity of step 6

The first point is addressed first by following the study of Liang et al. [11], the Jacobian of the system is considered to have a linear form with respect to the concentration vector:

$$\mathbf{J} = \begin{bmatrix} -(l_1 + l_4) & l_2 & l_3 & l_7 & 0 \\ l_1 & -l_2 & 0 & 0 & 0 \\ l_1 & l_2 & -l_3 & 0 & 2l_8 \\ l_4 & 0 & 0 & -l_7 - 4l_6 & 0 \\ 0 & 0 & 0 & l_7 + 2l_6 & -l_8 \end{bmatrix}. \tag{8}$$

This expression need an approximate value of the concentration of HO_2 denoted $C^*_{HO_2}$ (later explicited (10)) throught $l_6 = k_6 C^*_{HO_2}$. λ, which now denoted the largest eigenvalue of the linearized Jacobian J, can be obtained analytically following the same strategy as the one developed in [2], and is now time-dependent. This does not raise difficulties since the previous model described in [1] already needed $\dot{\omega}_\eta$ to be compute at every time-step, which becomes:

$$\dot{\omega}_\eta = \left[\lambda\left(C^*_{HO_2}\right) C_\eta + \epsilon_\eta\right] W_\eta. \tag{9}$$

The case presented in Figure 2.b is now performed with the integration of Eq.(9) in Figure 3. This time the evolution of C_η follows closely the one of C_{HO_2} until the thermal runaway. Since reaction 6 is only important in the low-temperature regime, where $C_\eta \approx C_{HO_2}$, the simple expression

$$C^*_{HO_2} = \frac{C_\eta}{1 + \alpha}, \tag{10}$$

will be used to evaluate $\mathbf{J}$ and λ for the rest of the paper. Other expression satisfying $\lim_{\alpha\to 0} C^*_{HO_2} = C_\eta$ and $\lim_{\alpha\to\infty} C^*_{HO_2} = 0$ can be used.

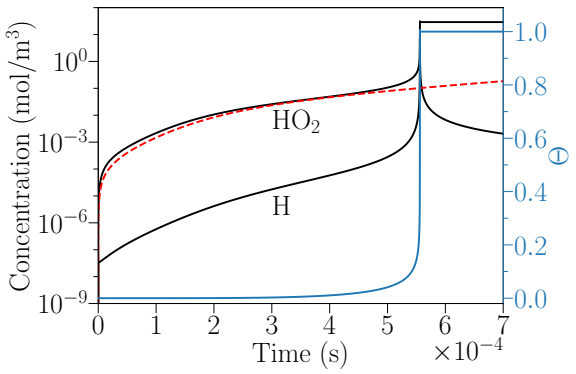

Figure 3: Normalized temperature (blue line, right axis), H and HO_2 concentrations (black lines, left axis) as functions of time, during isobaric homogeneous ignition processes from numerical integration with the 8-step skeletal chemistry for φ=1.0, with T_0=1100 K < T_c and p=50 atm. C_η is also presented (red dashed) using Eq. 9 with the reaction 6 linearization .

3.2. Low temperature thermal-runaway

The HO_2 concentration can now be predicted efficiently and accurately with the modifications of the previous subsection. We need to focus now on the thermal-runaway phenomenon, mainly caused by

the creation of H_2O, to model properly the ignition process [5, 10]. H_2O is only present in the 8-step mechanism through reaction 3:

$$\omega_{H_2O} = \frac{dC_{H_2O}}{dt} = l_3 C_{OH}. \tag{11}$$

To obtain a usable expression, we first need to assume H and O in quasi-steady-state, in addition, asymptotic analysis of the thermal runaway below crossover [5, 10] showed that HO_2 may also be assumed to be in steady state during the thermal runaway, leading to:

$$\omega_{H_2O} = 2k_6 C^{*2}_{HO_2}. \tag{12}$$

The heat released is mainly due to the production of H_2O (H_2 and O_2 having zero formation enthalpy), and reads:

$$\frac{dT}{dt} = \frac{-2k_6 \Delta H^0_{H_2O}}{\rho c_p} C^{*2}_{HO_2}, \tag{13}$$

with $\Delta H^0_{H_2O}$ the standard enthalpy of formation of gaseous H_2O, while ρ and c_p are the fresh gas density and specific heat at constant pressure.

In order to model the process leading to the thermal runaway we assume a single equivalent activation energy for λ in the low-temperature range with the introduction of a dimensionless activation energy β (to be explicited in Eq. (18)) and temperature θ:

$$\lambda(\theta) = \lambda e^{\theta}, \quad \theta = \beta \frac{T - T_0}{T_0}. \tag{14}$$

The thermal runaway problem can now be expressed following [5]:

$$\begin{cases} \dfrac{dC_\eta}{dt} = & C_\eta \lambda e^{\theta} \\ \dfrac{d\theta}{dt} = & q C_\eta^2 \end{cases} \quad \text{with } q = \frac{-2k_6 \beta \Delta H^0_{H_2O}}{T_0 \rho c_p}. \tag{15}$$

Upon integration we found

$$\theta(C_\eta) = \ln\left(1 + \frac{q C_\eta^2}{2\lambda}\right). \tag{16}$$

By injecting (16) in (14), we finally obtained the modified reaction rate $\dot{\omega}_\eta$

$$\dot{\omega}_\eta = \left[\lambda\left(C^*_{HO_2}\right) C_\eta + \frac{q}{2} C^{*3}_{HO_2} + \epsilon_\eta\right] W_\eta. \tag{17}$$

The thermal runaway is taken into account through the cubic term, that only corrects the scalar reaction rate below crossover since $C^*_{HO_2}$ will tend to zero in the high-temperature regime. This expression can therefore be used in both regimes.

Equation (16) needs the dimensionless activation energy β to be fully explicit. Because of the complex dependency on the temperature of λ, we choose to fit it only in the low-temperature regime, leading to:

$$\beta = \frac{35038}{T} - 2.54. \tag{18}$$

At 800K, β is over 40, enough to perform the high activation energy asymptotic analysis. Figure 4 presents the ignition histories obtained by now including the cubic correction term, for the same conditions as in Figure 3. The ignition process is now accurately recovered, even with just a single self-reacting scalar without any heat release. In addition, the temperature can be reconstructed from Eq. (16) and (14), as shown by the dashed green line in Fig. 4, which display a very good agreement during the thermal runaway.

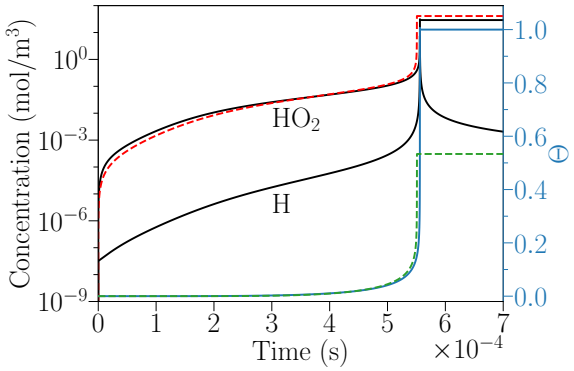

Figure 4: Normalized temperature (blue line, right axis), H and HO_2 concentrations (black lines, left axis) as functions of time, during isobaric homogeneous ignition processes from numerical integration with the 8-step skeletal chemistry for φ=1.0, with T_0=1100 K < T_c and p=50 atm. C_η is also presented (red dashed) using Eq. 16 with the linearized reaction 6 and the cubic correction term.

In order to access the capability of the new scalar reaction rate, we compared ignition delays in perfectly stirred reactors at constant pressure predicted by the 8-step mechanism and the new model. The previous model presented in [1] is also used to highlight improvement below the crossover.

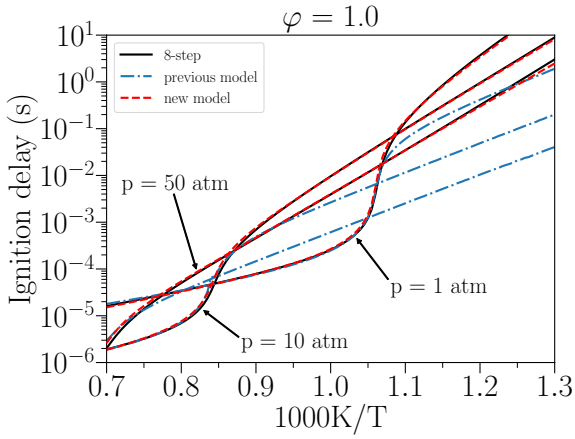

Figure 5: Comparison of ignition delays of an isobaric homogeneous ignition of an H_2-air mixture, obtained by numerical integration for the reduced 8-step chemistry (solid curves), the previous scalar model from [1] (blue dash-dotted curves) and the new scalar model (red dashed curve).

The ignition delays are shown in Fig. 5. The results predicted by the new model have an excellent agreement with the ones obtained using the reduced 8-step mechanism it has been based on, and that for the width range of temperature and pressure. Although it is not shown here, a similar agreement is obtained when varying the equivalence ratio and dilution.

3.3. Eigenvector based properties

After adjusting the reaction rate of the scalar to be valid for both above and below the crossover, it is crucial to adjust its diffusion coefficient. Indeed, the dominant radicals in the two regimes have significantly different diffusion properties. As a reminder, H (the main radical at high temperature) is 4 to 5 times more diffusive that the radicals found in the low-temperature regime (HO_2 and H_2O_2).

In order to overcome this problem, we can first realize that the eigenvector associated with λ gives us information about the molar proportion of the radical pool, and it can be obtained analytically:

$$\begin{cases} V_{\mathrm{H}} & = 1 \\ V_{\mathrm{O}} & = l_1 / (l_2 + \lambda)\, V_{\mathrm{H}} \\ V_{\mathrm{OH}} & = (l_1 V_{\mathrm{H}} + l_2 V_{\mathrm{O}} + 2 l_8 V_{\mathrm{H_2O_2}}) / (l_3 + \lambda) \\ V_{\mathrm{HO_2}} & = l_4 / (l_7 + 4 l_6 + \lambda)\, V_{\mathrm{H}} \\ V_{\mathrm{H_2O_2}} & = (l_7 + 2 l_6) / (l_8 + \lambda)\, V_{\mathrm{HO_2}}. \end{cases} \tag{19}$$

The eigenvector can then be used to model the diffusion coefficient of the scalar with a simple weighted average:

$$D_\eta = \sum_{k=1}^{5} D_k V_k / \sum_{k=1}^{5} V_k. \tag{20}$$

The benefit of using this expression is that it provides a diffusion coefficient that is both continuous, which is important for maintaining numerical stability, and representative of the radical pool. To demonstrate the impact of the diffusion properties of the scalar, a temporal mixing layer simulation was performed with the reduced 8-step chemistry and the new scalar model for different choices of its diffusion coefficient. This simple test case is made of a one-dimensional domain of 2 cm, divided into 500 points. Initially, the first half of the domain is filled with Air, while the second half is filled with diluted hydrogen (with 75% of N_2 in volume). The domain is initialized with a temperature of 1000 K and a pressure of 1 atmosphere. Simulations were performed using the hybrid Lattice Boltzmann solver used in Taileb et al. study [1].

The evolutions of the maximum concentrations of H, HO_2 and H_2O are reported in Figure 6, to highlight the importance of the scalar diffusion properties. The results clearly show that a carrier with slow diffusion (HO_2) leads to faster ignition (with a faster global rate), while a highly diffusive carrier such as H significantly slows down the process. In this particular case, the difference between the auto-ignition time with the two extremes diffusion coefficient choices is up to 13% of the ignition time obtained using the reduced 8-step chemistry. Using the weighted average based on the main eigenvector for the scalar diffusion property appears to be satisfactory, as it produces an accurate ignition growth rate (and hence an accurate delay).

4. TURBULENT MIXING LAYER VALIDATION

We will now evaluate the performance of the scalar model on a more challenging test case. It involves a two-dimensional turbulent double mixing layer, which was adapted from [12] to simulate high-pressure conditions. The domain is a 4.5 mm square that has been discretized using 500×500 points. To create the double mixing layer, we initially filled the first and last quarters of the domain along the x axis with

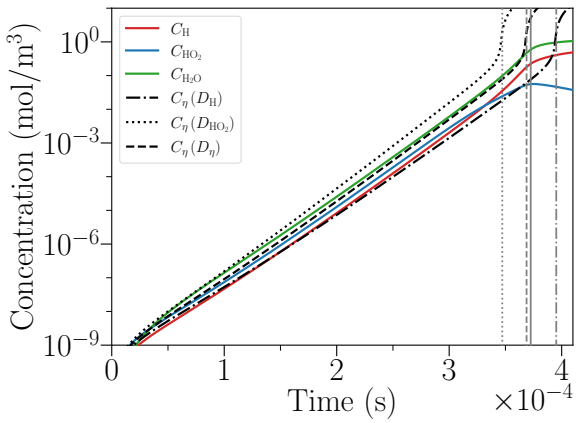

Figure 6: Evolution of the maximal (in the domain) concentration of the radicals for a temporal mixing layer (continuous curves). The evolution of the maximal value of the scalar is displayed (discontinuous black curves) for different diffusion coefficients used. The time of ignition is also displayed (vertical grey lines) for each case.

Air at a temperature of 1200 K, while the remaining half of the domain was filled with a H_2-N_2 mixture (50-50 in volume) at a temperature of 300 K. The pressure was set at 50 atmospheres to simulate hydrogen storage conditions. To emphasize the influence of chemistry modelling, we initialized the velocity field to be weakly turbulent. The turbulent field was generated using Rogallo's procedure [13] with a Passot-Pouquet spectrum [14]. We used a turbulent length scale of 0.45 mm and a root mean square of the velocity fluctuations of 0.70 m/s, which gave a turbulent time scale of 0.64 ms.

We used this particular configuration to compare the growth of ignition kernels under different chemical models. Specifically, we compared the San Diego mechanism, the reduced 8-step chemistry, the previous scalar model [1] (using the most relevant diffusion properties for these conditions, i.e., HO_2) and our current updated scalar model, which incorporates the average diffusion coefficient as described in equation (20). The recorded time of the first ignition event is presented in Table 2, along with the reduced time to solution and a normalised computational cost index. Notably, the updated scalar model reduces CPU cost by a factor of 43.7 compared to full chemistry integration. It is worth noting that all four simulations were performed on a dual CPU desktop (2 × Intel Xeon(R) Silver 4214R) with 20 cores.

Table 2: Summary of the auto-ignition time τ_i, the reduced time to solution RTTS (total CPU time in ms needed to simulate 1 ms for 1 cell) [15] and the cost (reduced time to solution with respect to the one of the scalar) of the four cases.

case	τ_i	RTTS	cost
San Diego	0.497 ms	1048	43.7
8 step	0.472 ms	218	9.1
Previous model ($D_{\mathrm{HO_2}}$)	0.826 ms	24	1.0
New model (D_η)	0.464 ms	24	1.0

Figure 7 displays the temperature fields obtained from the reduced chemistry model and the approximation derived using equation (16) for the updated scalar model, at 4 μs after the first ignition events. This comparison allows us to qualitatively assess the new scalar model's ability to accurately identify where ignition events occur.

We now present the temporal evolution of HO_2 concentrations at the four ignition kernels identified in Figure 7. This quantitative analysis allows us to assess the performance of the two scalar models in

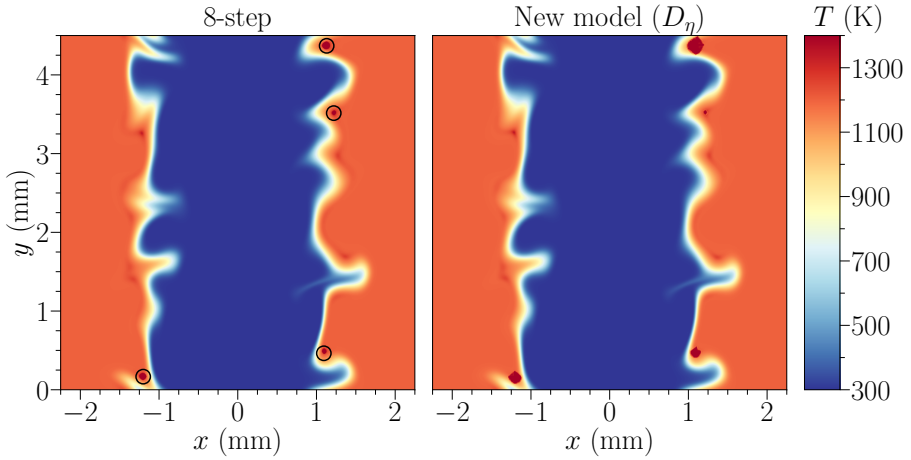

Figure 7: Comparison of the temperature fields obtained with the 8-step mechanism and with the new scalar model, taken 4 μs after the first ignition event. The four black circles identify the ignition kernels selected for Figure 8.

comparison with the detailed chemistry and the 8-step chemistry. The new scalar model formulation accurately reproduces the ignition behaviour of the reduced mechanism at a significantly lower computational cost. The differences between the new model and the detailed chemistry are primarily due to slight discrepancies between the detailed and 8-step mechanisms. In contrast, the previous scalar formulation [1] significantly overestimates ignition delays since it fails to consider the non-linearity of step 6 and thermal runaway.

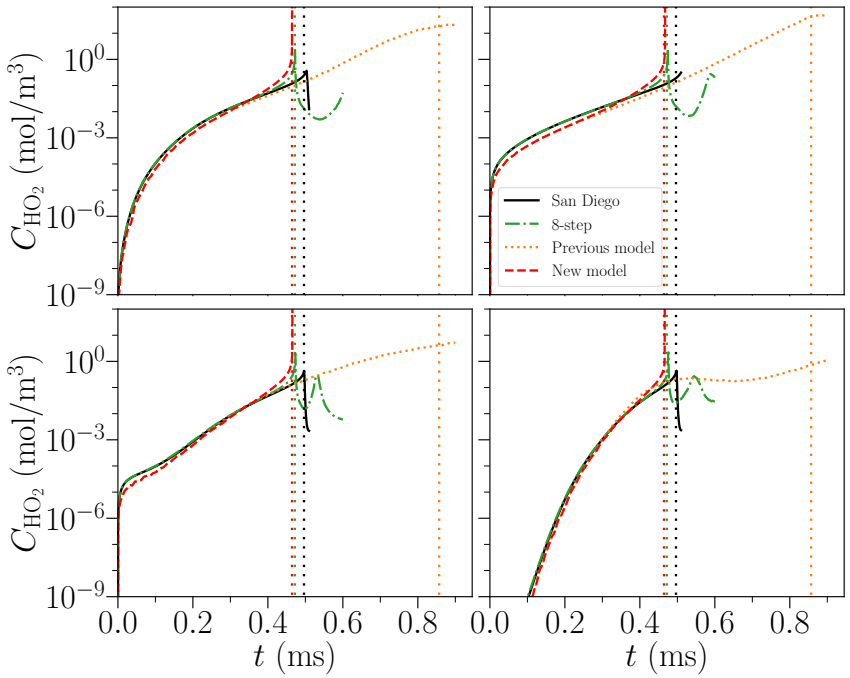

Figure 8: Evolution of the HO_2 concentrations at four positions of the mixing layer for reactive cases using the San Diego mechanism (black curve), the reduced 8-step (green dash-dotted curve), the previous scalar model (orange dotted curve) and the new scalar model (red dashed curve) using the averaged diffusion properties.

5. CONCLUSIONS

In summary, we have presented a new passive scalar model that can accurately predict ignition in complex flow configurations, building upon the previous model presented by Taileb et al. [1].

The new formulation is valid not only above the crossover temperature but also in its vicinity and in the low-temperature regime, making it particularly useful for high-pressure configurations commonly encountered in novel H_2 applications. We have achieved excellent accuracy by introducing three new elements to the model: an extended formulation of the branching characteristic time λ for the non-linear step 6, a cubic correcting term to account for thermal runaway, and a simple expression for the scalar diffusivity that considers the radical pool composition.

We have validated the model on various configurations, including homogeneous reactors, 1D temporal mixing layers, and a 2D DNS double mixing layer. In the future, we plan to extend the safety analysis to more complex configurations relevant to hydrogen storage. Overall, this work presents an important step towards developing a robust and efficient predictive model for ignition in hydrogen-based systems.

ACKNOWLEDGMENTS

Prof. Forman Williams is gratefully acknowledged for fruitful discussions on the scalar model formulation during summer 2022. Centre de Calcul Intensif d'Aix-Marseille, France and GENCI, France (Grant A0132B11951) are acknowledged for granting access to their high-performance computing resources. This research was supported by the MALBEC ANR, France project ANR-20-CE05-0009.

REFERENCES

1. S. Taileb, A. Millán-Merino, S. Zhao, and P. Boivin. Lattice-boltzmann modeling of lifted hydrogen jet flames: A new model for hazardous ignition prediction. *Combust. Flame*, 245:112317, 2022.
2. P Boivin, AL Sánchez, and FA Williams. Analytical prediction of syngas induction times. *Combust. Flame*, 176:489–499, 2017.
3. Bernard Lewis and Guenther Von Elbe. *Combustion, flames and explosions of gases*. Elsevier, 2012.
4. Antonio L. Sánchez and Forman A. Williams. Recent advances in understanding of flammability characteristics of hydrogen. *Prog. Energy Combust. Sci.*, 41:1–55, 2014.
5. Pierre Boivin, Antonio L Sánchez, and Forman A Williams. Explicit analytic prediction for hydrogen–oxygen ignition times at temperatures below crossover. *Combust. Flame*, 159:748–752, 2012.
6. Pierre Boivin, Marc Le Boursicaud, Alejandro Millan-Merino, Said Taileb, Josué Melguizo-Gavilanes, and Forman A. Williams. Hydrogen ignition and safety. In *Hydrogen for future thermal engines*. Springer, 2022.
7. FA Williams et al. Chemical-kinetic mechanisms for combustion applications, University of California, San Diego. version 2016-12-14, last accessed on 2023-02-22.
8. C. Treviño. Ignition phenomena in h_2-o_2 mixtures. *Progress in Astronautics and Aeronautics, AIAA*, 131:19–43, 1991.
9. G. Del Alamo, F.A. Williams, and A.L. Sanchez. Hydrogen-oxygen induction times above crossover temperatures. *Combust. Sci. Technol.*, 176:1599–1626, 2004.
10. Antonio L Sánchez, Eduardo Fernández-Tarrazo, and Forman A Williams. The chemistry involved in the third explosion limit of H_2-O_2 mixtures. *Combust. Flame*, 161:111–117, 2014.
11. Wenkai Liang and Chung K Law. An analysis of the explosion limits of hydrogen/oxygen mixtures with nonlinear chain reactions. *Phys. Chem. Chem. Phys.*, 20:742–751, 2018.
12. Hong G. Im, Jacqueline H. Chen, and Chung King Law. Ignition of hydrogen-air mixing layer in turbulent flows. *Symp. (Int.) Combust.*, 27:1047–1056, 1998.
13. Robert Sugden Rogallo. Numerical experiments in homogeneous turbulence. Technical Report NASA-TM-81315, NASA Ames Research Center, 1981.
14. Thierry Passot and Annick Pouquet. Numerical simulation of compressible homogeneous flows in the turbulent regime. *J. Fluid Mech.*, 181:441–466, 1987.
15. Abouelmagd Abdelsamie, Ghislain Lartigue, Christos E. Frouzakis, and Dominique Thévenin. The taylor–green vortex as a benchmark for high-fidelity combustion simulations using low-mach solvers. *Comput. Fluids*, 223:104935, 2021.